Title	An Almahata Sitta EL3 fragment: implications for the complex thermal history of enstatite chondrites
Authors	M. Kimura, M. K. Weisberg, A. Takaki, N. Imae, A. Yamaguchi
Citation	Progress in Earth and Planetary Science, 8(55), 1-12, 2021
Issue Date	2021-10-2
Type	Journal Article
URL	https://doi.org/10.1186/s40645-021-00447-2
Right	
Textversion	publisher

RESEARCH ARTICLE

An Almahata Sitta EL3 fragment: implications for the complex thermal history of enstatite chondrites

M. Kimura[1,2]*, M. K. Weisberg[3,4], A. Takaki[2], N. Imae[1,5] and A. Yamaguchi[1,5]

Abstract

Almahata Sitta is a polymict breccia, consisting of many kinds of clasts. Here we present our mineralogical and petrological results on an EL3 fragment, MS-177 from Almahata Sitta. This fragment shows a typical type 3 chondritic texture, consisting of well-defined chondrules, isolated silicate minerals, and opaque nodules. Most chondrules are enstatite-rich with some having olivine. Although these components are typical of EL3 chondrites, the mineral abundances and compositions are different from the other EL3s. Diopside is unusually abundant in MS-177. On the other hand, perryite and daubreelite were not found. The major pyroxene is orthoenstatite, and the silica phase is quartz. Fe–Ni metal has relatively high P contents. Troilite is enriched in Cr and Mn. Keilite and buseckite are present in MS-177. From the mineralogy and texture, MS-177 experienced a high-temperature event under subsolidus conditions. Shock-induced heating for a short duration might explain this high-temperature event. We suggest that other E3 chondrites also experienced heating events under such subsolidus conditions on their parent bodies. On the other hand, the high abundance of diopside cannot be explained by a secondary thermal event and may have been a primary feature of MS-177, formed before accretion to the parent body.

Keywords: Enstatite chondrite, Breccia, Thermal history, Opaque minerals

1 Introduction

Almahata Sitta fell in northern Sudan on October 7, 2008 and is a remarkable polymict breccia consisting of various ureilitic and chondritic fragments (e.g., Bischoff et al. 2010a, b; Horstmann and Bischoff 2014). The chondritic fragments include enstatite (E), ordinary, carbonaceous, and R-like chondrites. E chondritic fragments include EH3-6, EL3-6, and impact melt rocks. Here, we present a mineralogical and petrological study of the E chondrite fragment MS-177, which is classified as an EL3 (Hain, 2012; El Goresy et al. 2012).

Many studies have been conducted on not only EL3 but EH3 chondrites, to understand their complex thermal histories. Lin and El Goresy (2002) and Horstmann

et al. (2014) suggested that opaque nodules preserve evidence of variable thermal histories prior to accretion to the parent body, such as gas–solid condensation and melting. On the other hand, Zhang and Sears (1996) and Weyrauch et al. (2018) suggested that geothermometers for E3-6 chondrites do not always reflect their petrologic type. Rubin et al. (1997) showed that some E3 chondrites experienced heavy shock effects (S3-5). Kimura et al. (2017) studied a heavily shocked EH3, Asuka (A) 10164. A 10164 has a shock vein containing coesite, indicating that it experienced shock pressures of 3–10 GPa at temperatures of 1000 °C. The host chondrite was also heated, between 700 and 1000 °C, during the shock event. All of these studies show that the thermal and shock histories of EL3 chondrites are very complicated.

We selected MS-177 for study because it experienced an unusual shock-induced thermal history and is important for elucidating the complicated thermal history of E

*Correspondence: kimura.makoto@nipr.ac.jp
[1] National Institute of Polar Research, Tokyo, Japan
Full list of author information is available at the end of the article

Kimura *et al. Prog Earth Planet Sci*   (2021) 8:55

Page 2 of 12

chondrites. El Goresy et al. (2012, 2017) studied opaque nodules in this fragment and in another fragment, MS-17. They discussed a condensation origin for the phases in the nodules, especially oldhamite and sinoite, in the early solar nebula. Here we focus on the parent body thermal history of MS-177. We compare the results from MS-177 with two other EL3 chondrites, Asuka (A) 881314 and the heavily shocked EH3 chondrite, A 10164 (Kimura et al. 2017).

It is difficult to evaluate the thermal histories of E chondrites, especially the subsolidus conditions, by studying their silicate minerals. We do not have the appropriate silicate geothermometers, except for silica polymorphs (Kimura et al. 2005). Instead, some of the opaque minerals typical of E chondrites have been used to give quantitative constraints on the physical conditions of their thermal histories (e.g., Zhang and Sears 1996; Lin and El Goresy, 2002; Horstmann et al. 2014; Kimura et al. 2017). In addition, Weyrauch et al. (2018) recently proposed that E chondrites (EH and EL) are divided into "a" and "b" subgroups, based on the compositions of their sulfide minerals, which are not dependent on petrologic type (i.e., thermal alteration). This classification is significant in providing hints for understanding the thermal histories of E chondrites. We studied the opaque minerals in MS-177 to help constrain its thermal history. We expect that these geothermometers can help constrain the complicated thermal history not only for this fragment but also other E chondrites.

2 Sample and experimental methods

We investigated a polished thin section (PTS) of the MS-177 (EL3) fragment from Almahata Sitta. For comparison, we also studied a PTS of a typical EL3 chondrite, A-881314, 51-1.

Back-scattered electron (BSE) images were obtained using the JEOL JSM-7100F field emission scanning electron microscope (FESEM) at the National Institute of Polar Research (NIPR). Mineral analyses were conducted using the JEOL JXA8200 electron-probe microanalyzer at NIPR with a focused (1–2 μm) beam. The beam currents used were 4 nA for glass, plagioclase, and silica, and 30 nA for pyroxene, olivine, and opaque minerals at 15 keV. The analytical and correction methods were the same as those described by Kimura et al. (2017). The X-ray overlaps of K_a on K_b lines of some elements, Fe–Co and Ni–Cu, were corrected with a deconvolution program. We identified some phases using a laser micro Raman spectrometer (JASCO NRS 1000) at the NIPR after the method of Kimura et al. (2017). The elemental X-ray maps of the section were obtained using the FESEM. We determined modal abundances from elemental maps of the whole areas of the PTS. ImageJ software was used to calculate the modal abundances of minerals based on the X-ray intensities of each pixel. Imae et al. (2019) applied an X-ray diffraction (XRD) method to characterize minerals in meteorite sections by using SmartLab, RIGAKU at the NIPR. We used the same method for the identification of pyroxene in the sample studied here.

3 Results

3.1 Petrography

Figure 1a–d show the section of MS-177 studied here. MS-177 contains abundant, sharply bounded chondrules of spherical to ellipsoidal shapes, opaque nodules and isolated minerals. The fine-grained matrix is a minor component and not easily discernible like in other E3 chondrites (e.g., Weisberg and Kimura 2012). The texture of MS-177 is indicative of a type 3 E chondrite, which is supported by the occurrence of olivine in some chondrules (Weisberg and Kimura 2012; Weyrauch et al. 2018). The opaque minerals in MS-177 are typical of E chondrites, such as Si-bearing Fe–Ni metal and a (Mg,Mn,Fe)S phase (Weisberg and Kimura 2012).

Chondrules show well-defined outlines and are 0.69 mm in average diameter, typical of EL3 chondrites (0.6 mm) (e.g., Jones 2012). Most chondrules are porphyritic (pyroxene-dominated) and a few radial pyroxene types are present. Porphyritic chondrules mainly consist of low-Ca pyroxene phenocrysts and a devitrified mesostasis consisting of fine-grained high-Ca pyroxene and plagioclase, commonly with a silica phase. Olivine, when present, is generally poikilitically enclosed within pyroxene phenocrysts. One of the characteristic features of MS-177 is a high abundance of high-Ca pyroxene in the chondrules (Figs. 1c and 2a). It is generally not a common mineral in E3 chondrites. In chondrules of MS-177, high-Ca pyroxene occurs as coarse-grained phenocrysts, as rims on low-Ca pyroxene phenocrysts, and as fine-grained laths associated with plagioclase in chondrule mesostases. Fe–Ni metal and troilite with small amounts of a (Mg,Mn,Fe)S phase, oldhamite, and an (Fe,Zn)S phase are present in some chondrules. Isolated silicate minerals include low-Ca pyroxene, high-Ca pyroxene, plagioclase, and a silica mineral.

Opaque minerals in nodules and as isolated grains are mainly Fe–Ni metal with troilite and rare schreibersite (bright grains in Fig. 1d). Fe–Ni metal in the opaque nodules includes abundant euhedral laths of pyroxene (both low and high-Ca pyroxenes) with plagioclase and the oxynitride sinoite (Si_2N_2O; Fig. 2b). Oldhamite and the (Mg,Mn,Fe)S phase are rare in the nodules.

MS-177 shows some features generally interpreted to be shock-induced, such as undulose extinction, presence of irregular fractures in pyroxene and olivine, rare planar fractures in pyroxene, and rare sulfide veins. We could
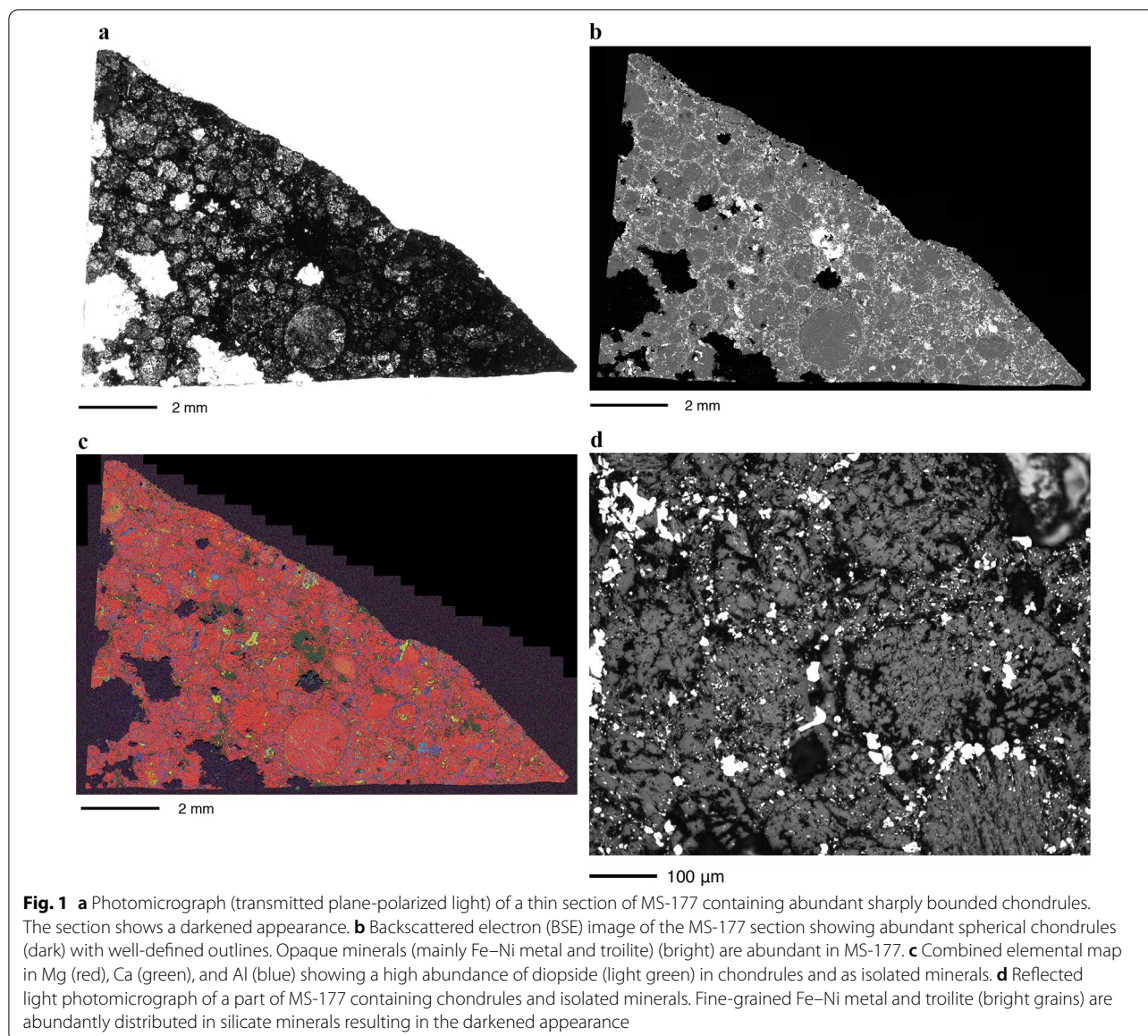
Kimura *et al. Prog Earth Planet Sci*   (2021) 8:55

Page 3 of 12

Fig. 1 a Photomicrograph (transmitted plane-polarized light) of a thin section of MS-177 containing abundant sharply bounded chondrules. The section shows a darkened appearance. **b** Backscattered electron (BSE) image of the MS-177 section showing abundant spherical chondrules (dark) with well-defined outlines. Opaque minerals (mainly Fe–Ni metal and troilite) (bright) are abundant in MS-177. **c** Combined elemental map in Mg (red), Ca (green), and Al (blue) showing a high abundance of diopside (light green) in chondrules and as isolated minerals. **d** Reflected light photomicrograph of a part of MS-177 containing chondrules and isolated minerals. Fine-grained Fe–Ni metal and troilite (bright grains) are abundantly distributed in silicate minerals resulting in the darkened appearance

not observe undulose extinction of plagioclase because of its small grain size. However, the plagioclase is not maskelynite, as discussed below, and mosaicism of pyroxene was not observed. All these features indicate that the shock stage of MS-177 is S2-3, after Rubin et al. (1997).

We found neither melt pockets nor melt veins in MS-177. The latter was reported in the heavily shocked A 10164 EH3 chondrite (Kimura et al. 2017). Euhedral laths of enstatite typical of melt rocks (Rubin and Scott 1997; Lin and Kimura 1998; Kimura and Lin 1999) were not found in MS-177, except in the opaque nodules, which is a characteristic of most EL3 chondrites

regardless of shock stage. Figure 2c shows the texture of metal and troilite as isolated minerals. They do not show a eutectic intergrowth texture, which is commonly present in a shock melt veins in A 10164 (Kimura et al. 2017). Fagan et al. (2000) reported shock-induced features in an EL chondrite, RKP 80249, such as enstatite prisms and opaque minerals in feldspathic glass. These features were not encountered in MS-177.

On the other hand, MS-177 shows darkening under plane polarized transmitted light (Fig. 1a) and reflected light (Fig. 1d) in the optical microscope. Many silicate phases contain abundant fine-grained opaque minerals resulting in the darkened appearance.
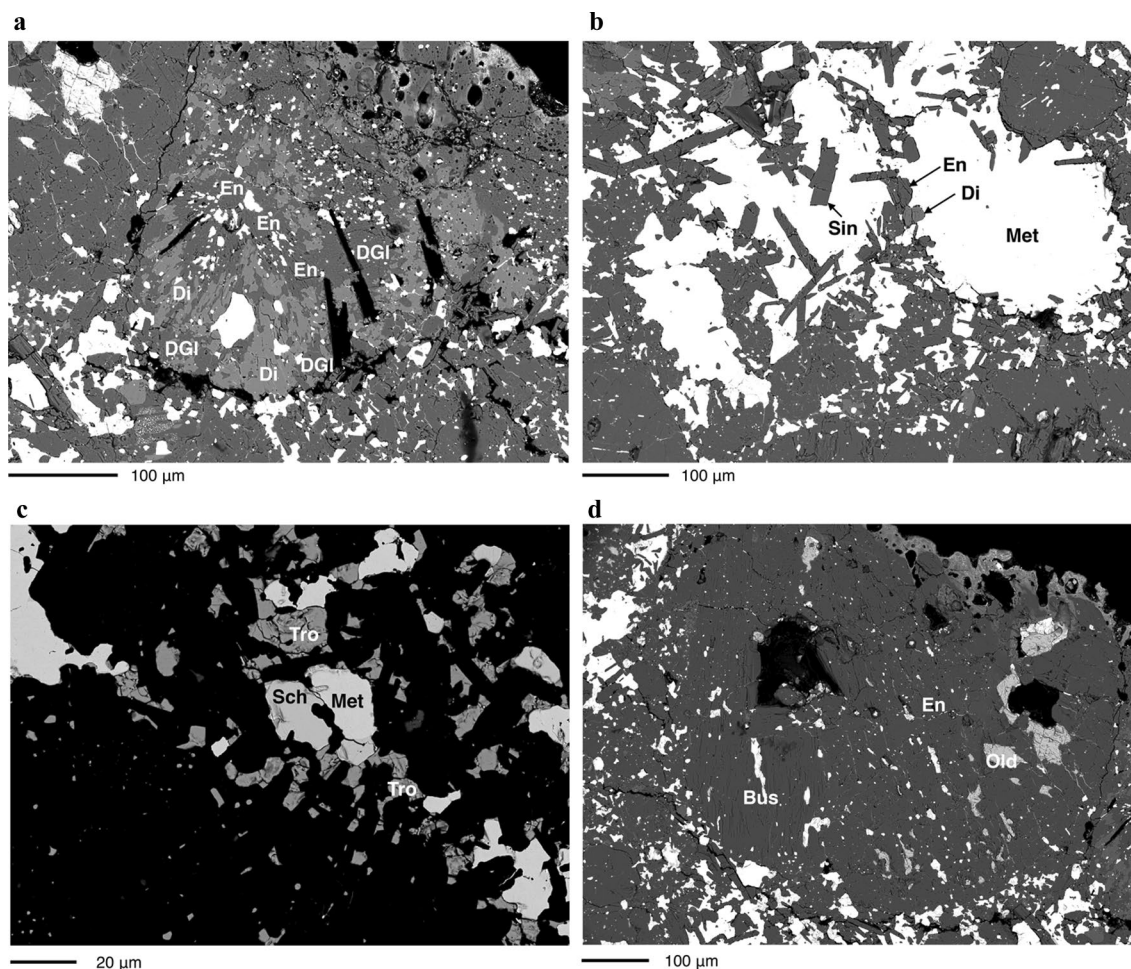
Kimura *et al. Prog Earth Planet Sci*   (2021) 8:55

Page 4 of 12

Fig. 2 BSE images of chondrules, an opaque nodule and metal from MS-177: **a** a chondrule consisting of abundant diopside (Di) with enstatite (En) and devitrified glass (DGl), in close association with abundant Fe–Ni metal (white). Black prismatic void spaces are encountered. **b** An opaque nodule consisting of Fe–Ni metal (Met) including laths of enstatite, diopside, and sinoite (Sin). **c** Isolated Fe–Ni metal, troilite (Tro), and schreibersite (Sch). **d** A chondrule mainly consisting of enstatite with oldhamite (Old) and buseckite (Bus)

3.2 Modal compositions

Table 1 shows the modal composition of the constituent minerals in MS-177 and average EL3 chondrite (Weisberg and Kimura 2012). The most abundant phase is low-Ca pyroxene (mostly enstatite), as is typical of EL chondrites. In comparison to the average EL3 (Weisberg and Kimura 2012), high-Ca pyroxene is highly abundant in MS-177, whereas olivine is not so abundant. Troilite is slightly more abundant than the average, but within the range of other EL3s. Schreibersite and the (Mg,Mn,Fe) S phase are slightly less abundant, and perryite and daubreelite were not found although they are typical minerals in EL chondrites.

3.3 Silicate mineral chemistry

Table 2 shows representative analyses of silicate minerals. Low-Ca pyroxene contains $Fs_{<1.3}$ and $Wo_{<1.4}$ components,

whereas high-Ca pyroxene is $Fs_{<1.4}$ and Wo_{43-48}. Hereafter we call them enstatite and diopside, respectively. FeO-rich low- and high-Ca pyroxene were not found in MS-177 or A-881314. Enstatite contains < 0.8 wt% Al_2O_3, and TiO_2; Cr_2O_3, and MnO are below detection limits (Table 3). Diopside contains < 0.2 wt% TiO_2, 0.2–1.1 Al_2O_3, < 0.13 Cr_2O_3, and < 0.12 MnO. In comparison, enstatite in the A-881314 EL3 contains $Fs_{<1.7}$ and $Wo_{<0.8}$, which is consistent with that in the MS-177 fragment. On the other hand, diopside was not found in A-881314.

Olivines, both in MS-177 and A-881314, are $Fa_{<1}$. They contain < 0.15 wt% MnO, whereas the other minor elements are below detection limits. FeO-rich olivine was not encountered in MS-177 or A-881314.

Plagioclases, both in MS-177 and A-881314, are enriched in the albite component, Ab_{61-74} and Ab_{63-91}, respectively. Devitrified glasses in chondrules of MS-177

Kimura *et al. Prog Earth Planet Sci*   (2021) 8:55

Page 5 of 12

Table 1 Modal composition (vol%) of the MS-177 and average EL3 chondrite

Mineral	MS-177	EL3 (average)
Enstatite	62.2	65.2
Diopside	3.4	0.3
Olivine	0.4	2.4
Plagioclase	13.6	10.4
Silica	0.7	1.1
Fe–Ni metal	9.4	10.1
Schreibersite	0.2	0.6
Perryite	n.i	0.1
Troilite	9.7	7.6
Oldhamite	0.3	0.6
Keilite–alabandite	trace	0.4
Daubreelite	n.i	0.3
Buseckite	trace	–
Sinoite	0.1	–

n.i. not identified, Weisberg and Kimura (2012)

contain 12.4–29.2 wt% Al_2O_3, 0.2–15.2 MgO, 0.8–13 CaO, 2.9–9.5 Na_2O, and 0.2–1.3 K_2O, indicative that they are mainly comprised of plagioclase and diopside

components. Some devitrified mesostasis glass contains up to 2.4 wt% Cl. El Goresy et al. (1988) also reported Cl in the mesostasis in chondrules in the Qingzhen EH3 chondrite. Chlorine-bearing phases were not identified in the chondrules from MS-177, such as djerfisherite, lawrencite, or hibbingite. Therefore, most chlorine is contained in the glassy mesostasis of MS-177 chondrules. The silica mineral in MS-177 is nearly pure SiO_2.

3.4 Opaque mineral chemistry

Table 3 shows representative analyses of the opaque minerals in MS-177. The Fe–Ni metal contains 0.3–0.6 wt% Si, which is within the range of A-881214 (Fig. 3a) and other EL chondrites, 0.4–1.0% (Weisberg and Kimura 2012). On the other hand, the metal contains 0.3–0.6 wt% P and 6.4–7.9 Ni, higher than in the metal of A-881314 (Fig. 3b). The Ni contents of metal in MS-177 are within the range of metal in other EL3 chondrites (Weisberg and Kimura, 2012), but the P contents are higher than in most other EL3 chondrites (<~0.1 wt%, unpublished data; Weisberg et al. 1995). This is one of the characteristic features of MS-177.

Schreibersite contains < 0.12 wt% Si and 7.0–7.8 wt% Ni. Although the Si contents are the same as those in

Table 2 Representative analyses of silicate phases (wt%)

Phase	Occurrence	SiO₂	TiO₂	Al₂O₃	Cr₂O₃	FeO	MnO	MgO	CaO	Na₂O	K₂O	Cl	Total	Fo/Wo/An	En/Ab	Fs/Or
Plagioclase	Chondrule	62.55	b.d	22.83	b.d	0.35	b.d	0.04	4.88	8.31	0.42	b.d	99.37	23.9	73.7	2.4
Glass	Chondrule	58.45	0.21	23.02	b.d	0.30	b.d	0.33	6.66	7.77	0.62	1.73	98.77			
Glass	Chondrule	63.51	b.d	19.69	0.07	b.d	b.d	7.31	4.24	6.15	0.50	0.15	101.64			
Olivine	Chondrule	42.63	b.d	b.d	b.d	0.06	0.15	56.60	b.d	b.d	b.d	b.d	99.44	99.9		
Diopside	Chondrule	56.05	0.05	0.24	0.07	0.39	0.09	19.03	24.51	0.11	b.d	b.d	100.54	47.8	51.6	0.6
Diopside	Isolated mineral	55.63	b.d	0.24	b.d	0.35	b.d	19.18	24.59	0.15	b.d	b.d	100.15	47.7	51.8	0.5
Enstatite	Chondrule	58.91	b.d	0.30	b.d	b.d	b.d	39.22	0.49	0.06	b.d	b.d	98.98	0.9	99.1	0.0
Enstatite	Isolated mineral	60.03	b.d	0.05	b.d	0.33	b.d	39.34	0.47	b.d	b.d	b.d	100.22	0.8	98.7	0.5
Quartz	Chondrule	96.62	0.07	0.10	b.d	0.13	b.d	0.10	0.08	0.13	b.d	b.d	97.22			

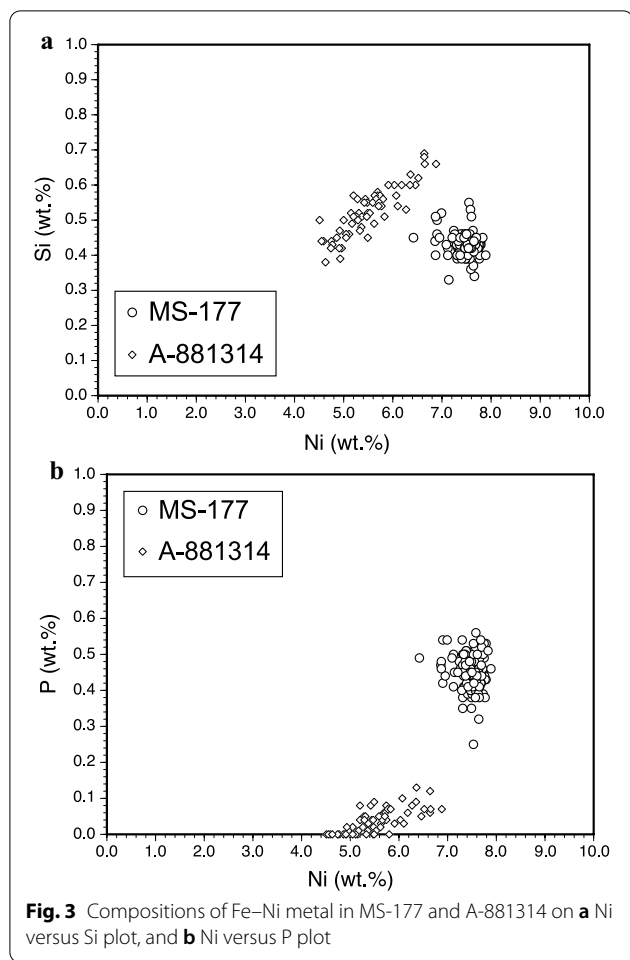b.d.: below detection limits (3σ), 0.03 for SiO₂, Al₂O₃, MgO, and CaO, 0.04 for TiO₂, Na₂O, and K₂O, 0.05 for FeO, Cr₂O₃, and Cl, and 0.08 for MnO

Table 3 Representative analyses of opaque minerals (wt%)

Phase	Occurrence	Mg	Si	P	S	Ca	Ti	Cr	Mn	Fe	Co	Ni	Cu	Zn	Total
Keilite	Chondrule	2.63	0.05	b.d	38.25	2.47	0.15	7.11	18.99	24.73	b.d	b.d	0.10	0.44	94.92
Fe–Ni metal	Chondrule	b.d	0.45	0.42	b.d	b.d	b.d	0.06	b.d	90.13	0.33	7.48	b.d	0.08	98.94
Fe–Ni metal	Isolated mineral	b.d	0.42	0.41	b.d	b.d	b.d	b.d	b.d	90.38	0.29	7.59	0.06	b.d	99.27
Oldhamite	Chondrule	0.61	0.20	0.04	40.90	53.28	b.d	b.d	1.19	0.77	b.d	b.d	b.d	b.d	96.99
Schreibersite	Isolated mineral	b.d	0.05	14.61	b.d	b.d	b.d	0.06	b.d	76.86	0.25	7.46	b.d	b.d	99.30
Buseckite	Chondrule	0.92	0.05	b.d	33.92	b.d	b.d	b.d	5.00	29.09	b.d	b.d	b.d	26.12	95.09
Troilite	Chondrule	0.08	b.d	b.d	36.40	b.d	0.32	2.41	1.33	57.58	b.d	0.20	0.07	b.d	98.40
Troilite	Isolated mineral	b.d	b.d	b.d	36.19	b.d	0.28	2.14	1.28	58.11	b.d	0.24	0.09	b.d	98.34

b.d.: below detection limits (3 s), 0.03 for Mg, Si, P, Ti, and Ca, 0.05 for S, Co, Ni, Cr, Mn, Fe, Zn, and Cu

The data of Fe–Ni metal and schreibersite as isolated mineral in this table are use to calculate geothermometries (see Text)
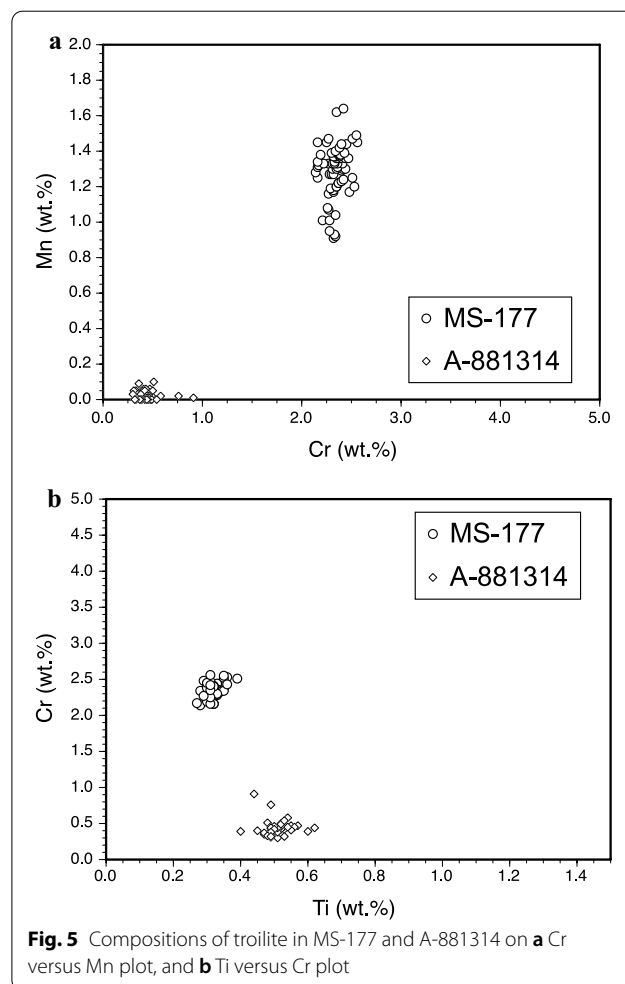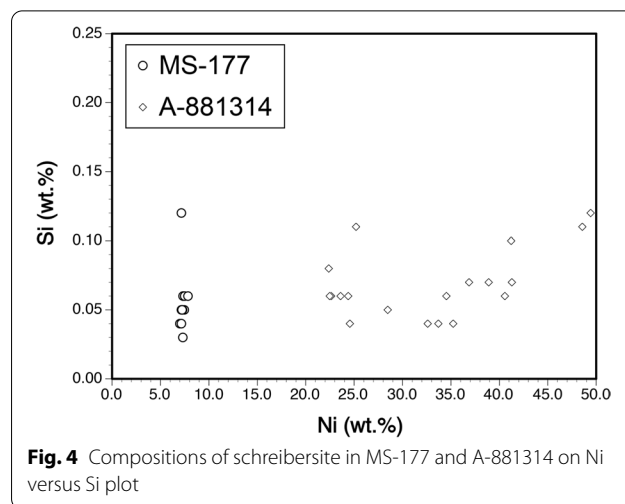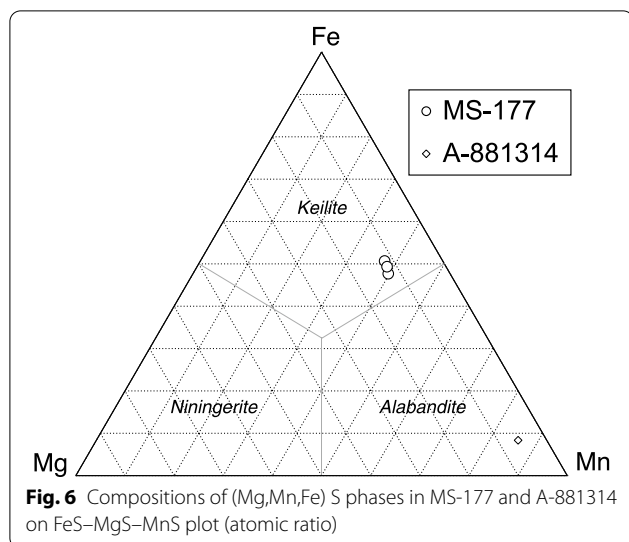
Kimura *et al. Prog Earth Planet Sci*   (2021) 8:55

Page 6 of 12

Fig. 3 Compositions of Fe–Ni metal in MS-177 and A-881314 on **a** Ni versus Si plot, and **b** Ni versus P plot

Fig. 4 Compositions of schreibersite in MS-177 and A-881314 on Ni versus Si plot

Fig. 5 Compositions of troilite in MS-177 and A-881314 on **a** Cr versus Mn plot, and **b** Ti versus Cr plot

A-881314 schreibersite, the Ni contents are much higher (Fig. 4).

Troilite contains 2.1–2.6 wt% Cr, 0.9–1.6 Mn, and 0.3–0.4 Ti. The Mn and Cr contents are higher than those in A-881314 troilite (Fig. 5a), whereas Ti contents are lower (Fig. 5b).

(Mg,Mn,Fe)S grains are rare in MS-177 (Table 3). Those found are identified as keilite, based on their compositions (Fig. 6). This is in contrast to the occurrence of alabandite in A-881314, which is a common mineral in EL chondrites (Weisberg and Kimura, 2012). Although the keilite contains 7.1 wt% Cr, daubreelite or other Cr-bearing phases were not observed in MS-177. Oldhamite is not common in MS-177 and contains 0.5–0.8 wt% Mg, 1.1–1.3 Mn, and 0.7–1.0 Fe.

An (Fe,Zn)S grain was found among enstatite grains in one chondrule (Fig. 2d). It contains 29.1 wt% Fe and 26.1 Zn. From the composition, the chemical formula of this phase is $(Fe_{0.49}Zn_{0.38}Mn_{0.09}Mg_{0.04})_{1.00}S_1$.

Fig. 6 Compositions of (Mg,Mn,Fe) S phases in MS-177 and A-881314 on FeS–MgS–MnS plot (atomic ratio)

3.5 Raman spectroscopy

Using laser Raman microscopy, we analyzed 9 feldspar grains and determined they are all plagioclase, based on the typical peaks of 506 and 206 cm^{-1} (Fig. 7a). They are not kumdykolite, a high-temperature polymorph of albitic plagioclase (Németh et al. 2013). Maskelynite or glass was not identified in any of the feldspars we analyzed. All of the silica (9 grains) is quartz, from the peak of 465 cm^{-1} (Fig. 7b), regardless of the textural setting. This is different from that in other EL3s in which the silica mineral is commonly tridymite or cristobalite (Kimura et al. 2005).

Figure 7c shows the Raman spectrum for the (Fe,Zn) S phase. The distinct peak of 300 cm^{-1} indicates that this is buseckite, and not rudashevskyite, a low-temperature polymorph of buseckite. This phase was first reported in an enstatite-rich achondrite, Zakłodzie, by Ma et al. (2012). To our knowledge, our finding is the second report of this mineral.

Fe–Ni metal contains sinoite grains which were identified by the peaks of 984, 734, 495, and 456 cm^{-1}, consistent with the peaks of sinoite in the Y-793225 E chondrite (Kimura et al. 2005).

3.6 XRD

We identified low-Ca pyroxene by XRD. The diffraction peaks of 321, 511, and 610 indices indicate that the dominant pyroxene is orthoenstatite, not clinoenstatite, in MS-177 (Fig. 8). Diopside (Dio) is also abundant, as identified from the XRD data.

4 Discussion

4.1 Classification

MS-177 was classified as an EL3 (Hain 2012; El Goresy et al. 2012). Our observations support this classification. The average diameter of the chondrules and Si contents in Fe–Ni metal and schreibersite are typical of EL chondrites. Although MS-177 experienced shock metamorphism (S2-3), it still preserves abundant well-defined chondrules with devitrified glassy mesostasis. These features are indicative of petrologic type 3. Chondrules also contain olivine. This is the key evidence for identification of type 3 E chondrites (e.g., Weisberg and Kimura 2012; Weyrauch et al. 2018).

Weyrauch et al. (2018) proposed that both EH and EL chondrites are divided into "a" and "b" subgroups based on their sulfide compositions, in spite of their petrologic type, since the compositions of sulfides do not depend on petrologic type. From their criteria, MS-177 is classified as an ELb3, based on the compositions of troilite enriched in Cr and Mn.

MS-177 has features that distinguish it from typical EL3 chondrites, including A-881314, such as occurrences of orthoenstatite, presence of quartz, and keilite, and absence of daubreelite. The high abundance of diopside is an especially unusual feature in comparison with any other E3 chondrite. In the following section, we discuss the unusual thermal history of MS-177.

4.2 Geothermometry

The thermal histories of meteorites have been addressed by mainly using silicate and oxide geothermometers. However, most of these thermometers cannot be applied to E chondrites because these minerals do not show solid solution in E chondrites. Instead, we use texture, mineral polymorphs, and opaque mineral features to elucidate the thermal history of the MS-177 EL3 fragment (Table 4).

MS-177 does not show evidence for shock-induced melting such as melt veins or pockets. The texture is different from those of melt rocks, as mentioned above. This suggests that the fragment did not experience heating higher than solidus temperature, < 1000 °C, after McCoy et al. (1999). The enstatite is identified as orthoenstatite, indicative of heating to temperatures > 600 °C, after Smyth (1974), assuming that enstatite in the chondrules and their fragments was initially clinoenstatite, as in the case of other type 3 E chondrites (Weisberg and Kimura 2012).

The absence of kumdykolite, a high-temperature polymorph of albitic plagioclase, indicates temperatures below ~ 1000 °C (Németh et al. 2013). The occurrence of quartz without tridymite, cristobalite or other polymorphs, suggests that equilibration temperatures were
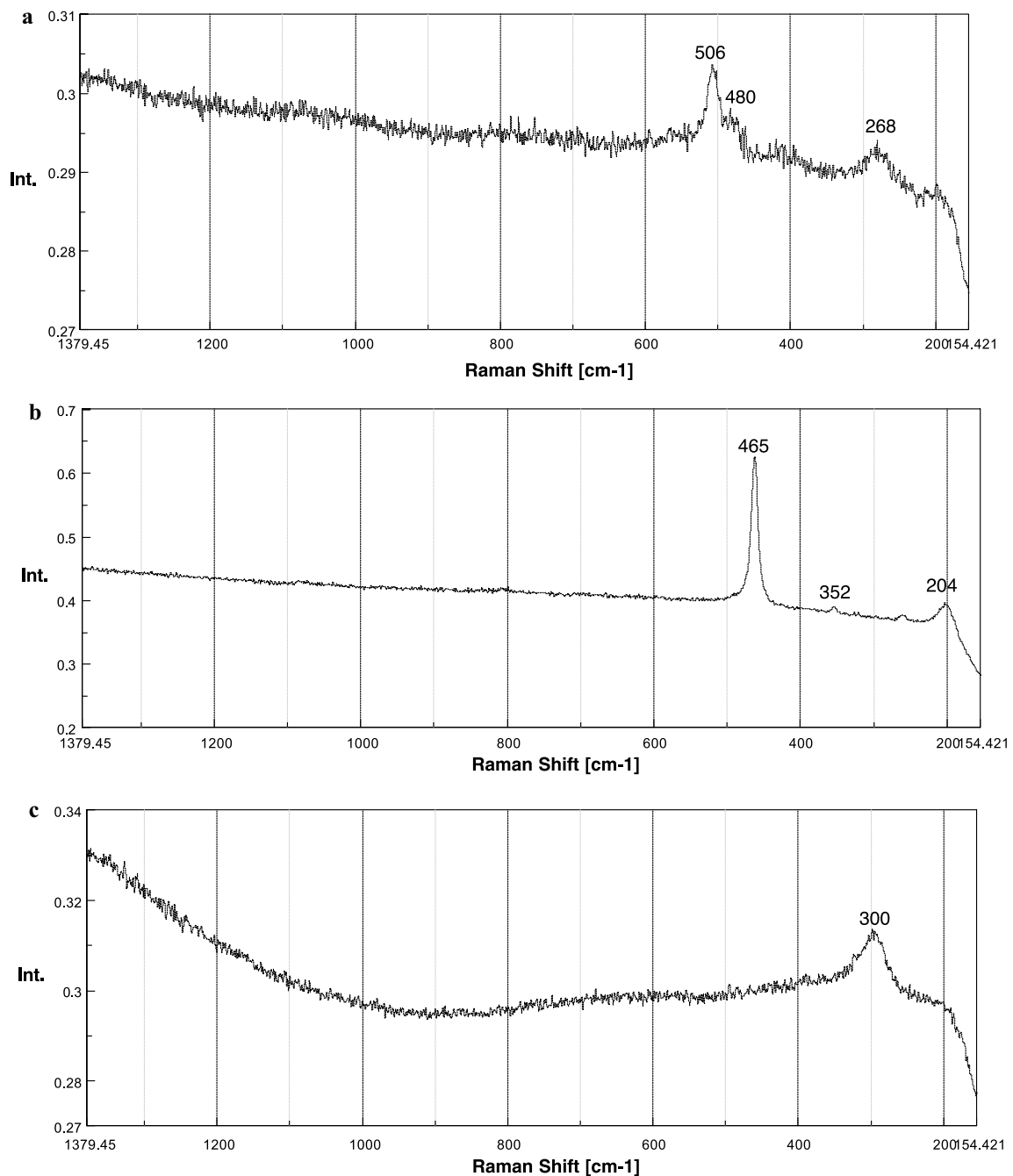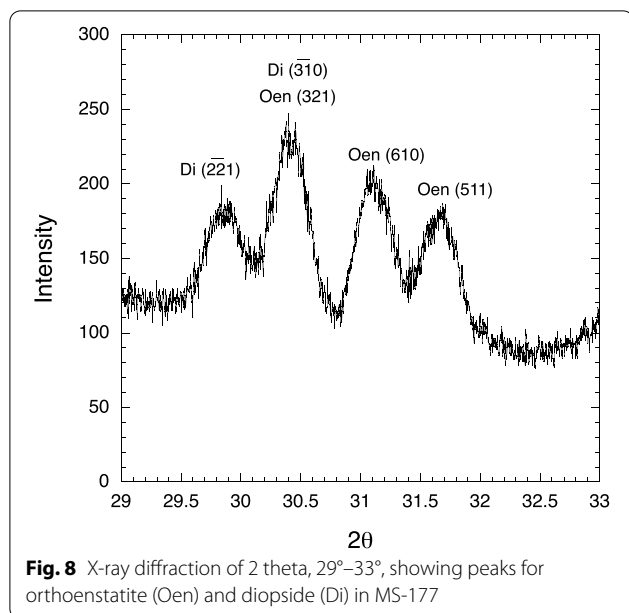
Fig. 7 Raman spectra of **a** plagioclase in a chondrule, **b** quartz in a chondrule, and **c** buseckite in a chondrule. All are from chondrules in MS-177

lower than 900 °C (Swamy et al. 1994). In the case of other type 3 E chondrites, the silica phases are generally cristobalite, tridymite, and glass, which crystallized from chondrule melts (Kimura et al. 2005). Therefore, the original silica phases in MS-177 were likely transformed into quartz during secondary heating below 900 °C.

Fe–Ni metal and troilite never show eutectic intergrowths, although they commonly occur in close association with each other. This observation indicates temperatures lower than eutectic melting, 970 °C (Ryzhenko and Kennedy 1973). This is consistent with the conclusions of El Goresy et al. (2017) who negated impact melting for the formation of metal nodules in

Kimura *et al. Prog Earth Planet Sci* (2021) 8:55

Page 9 of 12

Fig. 8 X-ray diffraction of 2 theta, 29°–33°, showing peaks for orthoenstatite (Oen) and diopside (Di) in MS-177

EL3 chondrites, based on their petrographic and isotopic features. Schreibersite is stable below 1000 °C (Doan and Goldstein, 1970). Coexisting metal and schreibersite (Table 3) indicates temperatures of ~ 850 °C, based on the partitioning of Ni between them, after Zhang and Sears (1996). Perryite was not found in MS-177. Although its stability is not yet known, it seems that the absence of perryite suggests high-temperature conditions (Kimura et al. 2005).

Troilite commonly contains relatively high Cr contents (Table 3; Fig. 5). This suggests high-temperature conditions of more than 700 °C (El Goresy and Kullerud, 1969). Under such conditions, daubreelite is not stable (El Goresy and Kullerud, 1969), and it was not found in MS-177.

The occurrence of keilite, not alabandite, also indicates high-temperature conditions. The composition (Table 3; Fig. 6) indicates ~ 600 °C for the keilite in MS-177, after Skinner and Luce (1971). Oldhamite contains ~ 2 mol% MgS and MnS components. This also suggests temperatures of ~ 600 °C (Skinner and Luce 1971). The occurrence of buseckite, not rudashevskyite, also supports high-temperature conditions (Ma et al. 2012), although the phase relationships between buseckite and rudashevskyite is not yet clear.

4.3 Thermal history

From the geothermometers discussed above and from petrographic observations, we discuss the unusual thermal history of MS-177. This fragment as well as A-881314 show typical type 3 E chondritic textures. However, the geothermometers indicate that MS-177 experienced a high-temperature event under subsolidus conditions, 600–850 °C. Horstmann et al. (2014) argued that metal-silicate intergrowths (opaque nodule in this paper) in EL3 chondrites did not form by impact melting. This is consistent with our temperature estimation. The temperature variation should reflect different closure temperatures of the different geothermometers. Nevertheless, we interpret the geothermometry to indicate that MS-177 experienced a high-temperature event. We suggest the heating event took place on the parent body because most minerals show similar high-temperature conditions, reflecting near-equilibrium conditions, as recorded by the geothermometry assessed in the previous section. This is different from other E3 chondrites where opaque nodules show different thermal histories in each E3 (Lin and El Goresy 2002). After the heating event, MS-177 cooled rapidly because both olivine and silica survive and primary

Table 4 Geothemometries

Phase	Geothermometry	References
Metal-Schreibersite	~ 850 °C	Zhang and Sears (1996)
Schreibersite	< 1000 °C	Doan and Goldstein (1970)
Perryite	High-temperature	Kimura et al. (2005)
Keilite	~ 600 °C	Skinner and Luce (1971)
Oldhamite	~ 600 °C	Skinner and Luce (1971)
Buseckite	High-temperature	Ma et al. (2012)
No daubreelite (Cr-bearing troilite)	≥ 700 °C	El Goresy and Kullerud (1969)
No metal-troilite eutectic intergrowth	< 970 °C	Ryzhenko and Kennedy (1973)
Quartz	< 900 °C	Presnell (1995)
Plagioclase (not kumdykolite)	< 1000 °C	Németh et al. (2013)
Orthoenstatite	> 600 °C	Smyth (1974)
No silicate melting	< 1000 °C	McCoy et al. (1999)

chondrule textures remain. None of the geothermometers we used indicate low-temperature conditions, supporting this conclusion. Therefore, the thermal history of MS-177 is different from equilibrated E chondrites which were heated for long durations, resulting in loss of well-defined chondrule boundaries and disappearance of olivine (e.g., Kimura et al. 2005).

The lower abundance of schreibersite in MS-177 than in A-881314 is consistent with the high Ni and P contents of the Fe–Ni metal, reflecting a high-temperature event. The low abundance of keilite is explained by the high concentration of Mn in troilite. The absence of daubreelite is consistent with our interpretation of the thermal history. Cr was mostly concentrated into the troilite under high-temperature conditions.

MS-177 contains a lower abundance of olivine than in other EL3 chondrites (Table 1). One possibility is that the olivine reacted with silica to form secondary enstatite under high-temperature conditions. However, we did not observe evidence of secondary enstatite. Poikilitic occurrence of olivine in enstatite phenocrysts indicates that some olivine survived without reaction with silica. Olivine is not very abundant in MS-177 and the abundance of silica is not different from that of other EL3s. Therefore, the low abundance of olivine is a primary feature of MS-177, although the possibility of olivine depletion through secondary reactions cannot be totally excluded.

In MS-177, diopside is highly abundant whereas oldhamite is rarely encountered. A possible explanation is that oldhamite reacted with silicate minerals to form diopside during a thermal event on the parent body. Fogel (1997) reported such metamorphic diopside in equilibrated E chondrites. However, diopside in MS-177 does not show the textures expected if it formed from secondary reactions in the parent body. Instead, diopside shows euhedral to subhedral morphologies in chondrules and opaque nodules, suggesting crystallization from the chondrule melts. Ikeda (1989) also reported that diopside crystallized in chondrules in Y-691, EH3 chondrite. A diopside-rich chondrule was reported in the MAC 88136 EL3 (Weisberg et al. 2012). Therefore, we conclude that the abundant diopside in MS-177 is a primary feature, present in chondrules and opaque nodules before their accretion onto the MS-177 parent body. This may be consistent with the pre-accretionary origin of opaque nodules in E chondrites, and not formation by an impact on the parent body (Hortsmann et al. 2014; Rindlisbacher et al. 2021). Horstmann et al. (2014) excluded a nebular origin for such nodules, from their trace element abundances. To further evaluate this possibility, we would need trace element data for the nodules in MS-177.

4.4 Formation process

In summary, the MS-177 EL3 fragment experienced secondary heating under subsolidus conditions on the parent body. The potential heat sources could be (1) internal heating by short-lived isotopes, such as ^{26}Al, as suggested for equilibrated O chondrites (e.g., Huss et al. 2006), (2) external heating such as solar-radiation and electromagnetic induction (Huss et al. 2006), and (3) shock-induced heating for short duration which is proposed for heated chondrites, such as in CM and CR chondrites (e.g., Kimura and Ikeda 1992; Nakato et al. 2008; Mahan et al. 2018). This may be related to the observation that many E3 chondrites experienced shock effect (mostly S3) (Rubin et al. 1997). As argued above, metamorphism for long duration by internal heating can be excluded for MS-177. The high temperatures induced by internal heating is long lasting, 10^6–10^8 years (Miyamoto et al. 1981). In this case, the texture of MS-177 should have become similar to those of E4-6 chondrites, in which recrystallization degrades chondrule boundaries and olivine disappears. Nevertheless, we cannot totally exclude the possibility that the parent body was disrupted into fragments during this high-temperature stage.

It is difficult to assess solar-radiation heating and electromagnetic induction as heat sources. We would need data for implanted solar-wind noble gases. MS-177 would have acquired implanted noble gases by the radiation on the parent body surface in the case of such heating. Additionally, it has been suggested that these heating mechanisms cannot supply enough energy to efficiently heat parent bodies (e.g., Huss et al. 2006).

On the other hand, MS-177 was shocked as suggested by the shock-induced features described above (and is S2-3). A 10164 also experienced a shock event (S4) and formed a melt vein. Not only the vein, but the host of A 10164 was heated during the shock event (Kimura et al. 2017). From the observation of A 10164 and the shock features of MS-177, shock-induced heating seems to be the most plausible heat source but not to the same degree as A 10164. The absence of high-pressure minerals suggests that the pressure conditions for MS-177 were low in comparison with A 10164, which experienced shock-induced partial melting under conditions of 3–10 GPa and 1000 °C (Kimura et al. 2017).

However, the post-shock temperature is not high in the case of shock stage S2-3. The post-shock temperature is estimated to be lower than 150 °C in ordinary chondrites (Fritz et al. 2017). If such temperatures can be applied to E chondrites, the estimated geothermometries outlined above give much higher temperatures than expected. If MS-177 experienced S5 stage, the temperature may be 600–900 °C (Fritz et al. 2017). However, mosaicism of pyroxene and melt pockets (or their relics), which are

indicative of S5 E and O chondrites (Rubin et al. 1997; Fritz et al. 2017), are not observed in MS-177. We also expect that such heavy shock would destroy the original type 3 texture of MS-177, through partial melting and vein formation (Rubin et al. 1997). Therefore, we conclude that MS-177 was not heavily shocked. It may have been buried beneath an impact crater or deposited in a hot eject blanket as suggested for annealed ordinary chondrites (Rubin, 2004) and was heated to the subsolidus temperatures mentioned above, for a short duration. Following this heating event, MS-177 experienced a shock event, resulting in its shock-induced features (of S2-3).

The duration of high-temperature conditions did not continue for a long time, and the primary texture and olivine enclosed in pyroxene survived. Thus, the thermal history of MS-177 is unusual, differing from the high temperature and pressure conditions for the heavily shocked A 10164, and the low-temperature conditions for A-881314 containing Fe-poor alabandite, Mn-Cr-poor troilite, and daubreelite. MS-177 is similar to subgroup b of E chondrites after Weyrauch et al. (2018). We suggest that these Eb chondrites and MS-177 experienced similar high-temperature conditions on their parent bodies, although the petrographic features, such as the primary texture, survived during the high-temperature event.

The Almahata Sitta meteorite came from the asteroid 2008 TC3. The formation of this brecciated asteroid is a controversial issue (e.g., Horstmann and Bischoff 2014). However, urelilitic and chondritic materials were assembled into the parent body, which was very loosely consolidated (Bischoff et al. 2010a, b). This may suggest that the fragments did not react with each other in the parent body. Therefore, the unusual thermal history of MS-177 originated before final accretion of the Almahata Sitta parent body and developed from the original E chondritic parent body.

5 Summary

We studied fragment MS-177 from the Almahata Sitta polymict breccia. MS-177 is classified as an EL3 chondrite based on petrographic observations and mineral chemistry. However, it shows mineralogical features, such as abundant diopside and lack of daubreelite, not observed in any other E3 chondrite. From the mineral chemistry, MS-177 is also classified as an ELb chondrite, based on the classification scheme proposed by Weyrauch et al. (2018). Several geothermometers that we used suggest that this fragment was subjected to a high-temperature event for a short duration, which is supported by the preservation of olivine and the primary texture. This may have resulted from a shock event. Enstatite chondrites, including type 3, experienced complicated formation processes including shock and thermal events. Some of them were subjected to high-pressure and temperature conditions like A 10164. Others were heated for short duration under subsolidus conditions like MS-177, or not metamorphosed like A-881314, in the parent body. These differences may reflect wide variation in the shock histories of the E chondrite parent bodies. E chondrites may have experienced a greater number of shock events than other chondrites (Rubin et al. 1997).

Authors' contributions
MK carried out the analyses and designed this study. MKW proposed this study. AT, NI, and AY analyzed the data. All authors read and approved the final manuscript.

Author details
[1]National Institute of Polar Research, Tokyo, Japan. [2]Ibaraki University, Mito, Japan. [3]Kingsborough College and Graduate Center of the City University of New York, New York, USA. [4]American Museum of Natural History, New York, USA. [5]SOKENDAI, Tokyo, Japan.

References
Bischoff A, Horstmann M, Pack A, Laubenstein M, Haberer S (2010a) Asteroid 2008 TC3—Almahata Sitta: A spectacular breccia containing many different ureilitic and chondritic lithologies. Meteorit Planet Sci 45:1638–1656

Bischoff A, Horstmann M, Laubenstein, M, and Haberer S (2010b) Asteroid 2008 TC3 ? Almahata Sitta: not only a ureilitic meteorite, but a breccia containing many different achondritic and chondritic lithologies (abstract #1763). 41st Lunar and planetary science conference

El Goresy A, Kullerud G (1969) Phase relations in the system Cr–Fe–S. In: Millman PM (ed) Meteorite research. D. Reidel, Dordrecht

El Goresy A, Yabuki H, Ehlers K, Woolum D, Pernicka E (1988) Qingzhen and Yamato-691: a tentative alphabet for the EH chondrites. Proc NIPR Symp Antarct Meteorites 1:65–101

El Goresy A, Lin Y, Feng L, Boyet M, Hao J, Zhang J, Dubrovinsky L (2012) Almahata Sitta EL-3 Chondrites: sinoite, graphite, and oldhamite (CsS) assemblages C- and N-isotopic compositions and REE patterns. In:

Kimura *et al. Prog Earth Planet Sci*   (2021) 8:55

Page 12 of 12

Abstracts of the 75th annual meeting of the meteoritical society, Cairns, Australia, 12–17 August 2012

El Goresy A, Lin Y, Miyahara M, Gannoun A, Boyet M, Ohtani E (2017) Origin of EL3 chondrites: evidence for variable C/O ratios during their course of formation—a state of the art scrutiny. Meteorit Planet Sci 52:781–806

Fagan TJ, Scott ERD, Keil K, Cooney TF, Sharma SK (2000) Formation of feldsphathic and metallic melts by shock in enstatite chondrite Reckling Peak A80259. Meteorit Planet Sci 35:319–329

Fogel RA (1997) On the siginificance of diopside and oldhamite in enstatite chondrites and aubrites. Meteorit Planet Sci 32:577–591

Fritz J, Greshake A, Fernandes VA (2017) Revising the shock classification of meteoites. Meteorit Planet Sci 52:1216–1232

Hain H (2012) Characterization of different meteorite samples from the Almahata Sitta strewn field. Bachelor Thesis, Institut für Planetologie, Westfälische Wilhelms-Universität Münster, Germany

Horstmann M, Bischoff A (2014) The Almahata Sitta polymict breccia and the late accretion of asteroid 2008 TC3. Chem Erde 74:149–183

Horstmann M, Humayun M, Bischoff A (2014) Clues to the origin of metal in Almahata Sitta EL and EH chondrites and implications for primitive E chondrite thermal histories. Geochim Cosmochim Acta 140:720–744

Huss GR, Rubin AE, Grossman JN (2006) Thermal metamorphism in chondrites. In: Lauretta DS, McSween HY Jr (ed) Meteorites and the Early Solar System. The University of Arizona Press

Ikeda Y (1989) Petrochemical study of the Yamato-691 enstatite chondrite (E3) III: descriptions and mineral compositions of chondrules. Proc NIPR Symp Antarct Meteorites 2:75–108

Imae N, Kimura M, Yamaguchi A, Kojima H (2019) Primordial, thermal, and shock features of ordinary chondrites: emulating bulk X-ray diffraction using in-plane rotation of polished thin sections. Meteorit Planet Sci 54:919–937

Jones RH (2012) Petrographic constraints on the diversity of chondrule reservoirs in the protoplanetary disk. Meteorit Planet Sci 47:1176–1190

Kimura M, Ikeda Y (1992) Mineralogy and petrology of a unusual Belgica-7904 carbonaceous chondrite: genetic relationships between the components. Proc NIPR Symp Antarc Meteorites 5:72–117

Kimura M, Lin Y (1999) Petrological and mineralogical study of enstatite chondrites with reference to their thermal histories. Antarct Meteor Res 12:1–18

Kimura M, Weisberg MK, Lin Y, Suzuki A, Ohtani E, Okazaki R (2005) Thermal history of the enstatite chondrites from silica polymorphs. Meteorit Planet Sci 40:855–868

Kimura M, Yamaguchi A, Miyahara M (2017) Shock-induced thermal history of an EH3 chondrite, Asuka 10164. Meteorit Planet Sci 52:24–35

Lin Y, El Goresy A (2002) A comparative study of opaque phases in Qingzhen (EH3) and MAC 88136 (EL3): representatives of EH And EL parent bodies. Meteorit Planet Sci 37:577–600

Lin Y, Kimura M (1998) Petrographic and mineralogical study of new EH melt rocks and a new enstatite chondrite grouplet. Meteorit Planet Sci 33:501–511

Ma C, Beckett JR, Rossman GR (2012) Buseckite, (Fe, Zn, Mn)S, a new mineral from the Zakłodzie meteorite. Am Miner 97:1226–1233

Mahan B, Moynier F, Beck P, Pringle EA, Siebert J (2018) A history of violence: insights into post-accretionary heating in carbonaceous chondrites from volatile element abundances, Zn isotopes and water contents. Geochim Cosmochim Acta 220:19–35

McCoy TJ, Dickinson TL, Lofgren GE (1999) Partial melting of the Indarch (EH4) meteorite: a textural, chemical, and phase relations view of melting and melt migration. Meteorit Planet Sci 34:735–746

Miyamoto M, Fujii N, Takeda H (1981) Ordinary chondrite parent body: an internal heating model. Proc Lunar Planet Sci Conf 12B:1145–1152

Nakato A, Nakamura T, Kitajima F, Noguchi T (2008) Evaluation of dehydration mechanism during heating of hydrous asteroids based on mineralogical and chemical analysis of naturally and experimentally heated CM chondrites. Earth Planets Space 60:855–864

Németh P, Lehner SW, Petaev MI, Buseck PR (2013) Kumdykolite, a high-temperature feldspar from an enstatite chondrite. Am Miner 98:1070–1073

Rindlisbacher MA, Weisberg MK, Ebel DS, Alpert SP (2021) Metal-rich nodules in anomalous EL3 chondrite Northwest Africa (NWA) 8785. Meteorit Planet Sci 56:960–970

Rubin AE (2004) Postshock annealing and postannealing shock in equilibrated ordinary chondrites: implications for the thermal and shock histories of chondritic asteroids. Geochim Cosmochim Acta 68:673–689

Rubin AE, Scott ERD (1997) Abee and related EH chondrite impact-melt breccias. Geochim Cosmochim Acta 61:425–435

Rubin AE, Scott ERD, Keil K (1997) Shock metamorphism of enstatite chondrites. Geochim Cosmochim Acta 61:847–858

Ryzhenko B, Kennedy GC (1973) The effect of pressure on the eutectic in the system Fe–FeS. Am J Sci 273:803–810

Skinner BJ, Luce FD (1971) Solid solutions of the type (Ca, Mg, Mn, Fe)S and their use as geothermometers for the enstatite chondrites. Am Miner 56:1269–1296

Smyth JR (1974) Experimental study on the polymorphism of enstatite. Am Miner 59:345–352

Swamy V, Saxena S, Sundman B, Zhang J (1994) A thermodynamic assessment of silica phase diagram. J Geophys Res 99:11787–11794

Weisberg MK, Kimura M (2012) The unequilibrated enstatite chondrites. Chem Erde 72:101–115

Weisberg MK, Ebel DS, Kimura M (2012) Petrology of chondrules and a diopside-rich inclusion in the MAC 88136 EL3 Chondrite. In: Abstracts of the 75th annual meeting of the meteoritical society, Cairns, Australia, 12–17 August 2012

Weyrauch M, Horstmann M, Bischoff A (2018) Chemical variations of sulfides and metal in enstatite chondrites-introduction of a new classification scheme. Meteorit Planet Sci 53:394–415

Zhang Y, Sears DWG (1996) The thermometry of enstatite chondrites: a brief review and update. Meteorit Planet Sci 31:647–655